Smoluchowski diffusion equation for active Brownian swimmers

Francisco J. Sevilla[1,*] and Mario Sandoval[2,†]
[1]*Instituto de Física, Universidad Nacional Autónoma de México, Apdo. Postal 20-364, 01000, México D.F., Mexico*
[2]*Department of Physics, Universidad Autonoma Metropolitana-Iztapalapa, Distrito Federal 09340, Mexico*
(Received 29 January 2015; published 29 May 2015)

We study the free diffusion in two dimensions of active Brownian swimmers subject to passive fluctuations on the translational motion and to active fluctuations on the rotational one. The Smoluchowski equation is derived from a Langevin-like model of active swimmers and analytically solved in the long-time regime for arbitrary values of the Péclet number; this allows us to analyze the out-of-equilibrium evolution of the positions distribution of active particles at all time regimes. Explicit expressions for the mean-square displacement and for the kurtosis of the probability distribution function are presented and the effects of persistence discussed. We show through Brownian dynamics simulations that our prescription for the mean-square displacement gives the exact time dependence at all times. The departure of the probability distribution from a Gaussian, measured by the kurtosis, is also analyzed both analytically and computationally. We find that for the inverse of Péclet numbers $\lesssim 0.1$, the distance from Gaussian increases as $\sim t^{-2}$ at short times, while it diminishes as $\sim t^{-1}$ in the asymptotic limit.

DOI: 10.1103/PhysRevE.91.052150 PACS number(s): 05.40.Jc, 05.10.Gg, 02.30.Jr

I. INTRODUCTION

The study of self-propelled (active) particles moving at small scales has received much attention [1–9]. This is because phenomena in nature, like the motion of plankton, viruses, and bacteria, have an important role in many biological processes as well as in industrial applications and, more generally, because active particles are suitable elements of analysis in the context on nonequilibrium statistical physics. Moreover, matter made by self-propelled particles has been observed to behave in very different ways compared to matter conformed by passive ones [10,11], mainly due to the out-of-equilibrium nature of active systems characterized by persistent motion. Hence, the search for analytical solutions of systems conformed of active particles, even in the simplest situations, as in the absence of boundaries or chirality, is of current interest.

From a technological point of view, the study of active particles is also very relevant. For example, the bioengineering community is constructing self-propelled micromachines [12,13] inspired by natural swimmers for the purpose of making devices able to deliver specialized drugs in precise regions inside the human body [14] or to serve as micromachines able to detect and diagnose diseases [15–17]. These microrobots, in the same way as the smallest microorganisms, are subject to thermal fluctuations or Brownian motion, which is an important effect to take into account, since thermal fluctuations make the particles lose their orientation, thus affecting the particles' net displacement. Most classical literature considering the effect of loss of persistence orientation, due to Brownian motion, on the diffusion of active particles has used a Langevin approach, since it can be considered a direct way of finding the particles effective diffusion. Within this approach, isotropic self-propelled bodies subject to thermal forces [5,18,19] and anisotropic swimmers [18] have been treated in the absence and presence of external fields [20–23].

A Smoluchowski approach to study the effective diffusion of active particles in slightly complex environments has also been undertaken. For example, Pedley [24] introduced a continuum model to calculate the probability density function for a diluted suspension of gyrotactic bacteria. Bearon and Pedley [25] studied chemotactic bacteria under shear flow and derived an advection-diffusion equation for cell density. Enculescu and Stark [26] studied, theoretically, the sedimentation of active particles due to gravity and subject to translational and rotational diffusion [27]. Similarly, Pototsky and Stark [28] followed a Smoluchowski approach and analyzed active Brownian particles in two-dimensional traps. Saintillan and Shelley [29] used a kinetic theory to study pattern formation of suspensions of self-propelled particles.

Self-propelled particles in nature move, in general, with a time-dependent swimming speed, like microorganisms that tend to relax (rest) for a moment and then to continue swimming [30]. In this work, we assume that particles move freely with a constant swimming speed, which is a simplified model that has been supported by experimental work [20,31] and has also been adopted when studying collective behavior [32]. Other more complex scenarios where, for example, active Brownian particles are subject to external flows, have been reported and solved following the Langevin approach [23].

In this paper we follow the approach of Smoluchowski and focus on the coarse-grained probability density of finding an active Brownian particle—that diffuses translationally and rotationally in a two-dimensional, unbounded space, and immersed in a steady fluid—at position $\boldsymbol{x}$ at time t without making reference to its direction of motion $\hat{\boldsymbol{u}}$. We derive, from Langevin's equations, the Smoluchowski's equation for such probability density and we solve it analytically.

Briefly, the Smoluchowski's equation is obtained by the use of Fourier analysis to translate the Fokker-Planck equation for active particles [see Eq. (3)] into a hierarchical infinite set of coupled ordinary differential equations for the Fourier coefficients (that simply correspond to the projections of the complete probability distribution, the one that depends explicitly on $\boldsymbol{x},\hat{\boldsymbol{u}}$, and t, onto the Fourier basis on the same support of the direction of motion, i.e., $[-\pi,\pi]$), where the

*fjsevilla@fisica.unam.mx
†sem@xanum.uam.mx

quantity of interest coincides with the Fourier coefficient corresponding to the lowest Fourier mode. The hierarchy is similar to that of Bogoliubov-Born-Green-Kirkwood-Yvon that appears in kinetic theories that use the Boltzmann equation. Clearly, any attempt to resolve the complete system is impractical, thus we analyze the consequences of a closure of the hierarchy at the second and third levels, at which we are able to provide explicit solutions for the probability density function (p.d.f.) that is of our interest. Subsequently, we transform back to the coordinate space, and we are able to explicitly find the p.d.f. of an active Brownian particle in the short- and long-time regimes. The *exact* time dependence of mean-square displacement (msd) for a swimmer is found, and classical results for the enhanced diffusion of an active particle are recovered. We also find theoretical results for the kurtosis of the swimmer, hence a discussion concerning the non-Gaussian behavior at intermediate times of an active swimmer p.d.f. is also offered. Finally, and for comparison purposes, simulations based on Brownian dynamics were also performed, and we obtained an excellent agreement among our theoretical and computational results.

II. THE MODEL

Consider a spherical particle of radius a, immersed in a fluid at fixed temperature T, that self-propels in a two-dimensional domain. The particle is subject to thermal fluctuations, $\boldsymbol{\xi}_T(t)$, which affects the translational part of motion, and to active fluctuations, $\xi_R(t)$, which affects the rotational one. Both kinds of fluctuations are modeled as white noise, i.e., $\langle \boldsymbol{\xi}_T \rangle = \langle \xi_R \rangle = 0$, $\langle \xi_{i,T}(t)\xi_{j,T}(s)\rangle = 2D_B\delta(t-s)\delta_{i,j}$ and $\langle \xi_R(t)\xi_R(s)\rangle = 2D_\Omega\delta(t-s)$, where the subscripts i,j denote the Cartesian components x, y, of a two-dimensional vector. Here $D_B = k_BT/6\pi\eta a$ and D_Ω are, respectively, the translational and rotational diffusivity constants, with η being the viscosity of the fluid.

The particle swimming velocity, $\mathbf{U}_s(t)$, is written explicitly as $U_s(t)\hat{\boldsymbol{u}}(t)$, where we denote by $\hat{\boldsymbol{u}}(t) = [\cos\varphi(t), \sin\varphi(t)]$ ($\varphi(t)$ being the angle between the direction of motion and the horizontal axis) the instantaneous unit vector in the direction of swimming and $U_s(t)$ the instantaneous magnitude of the swimming velocity along $\hat{\boldsymbol{u}}(t)$. Each of these quantities may be determined from its own dynamics [33], and Langevin equations for each may be written. Here we consider the case of a faster dynamics for the swimming speed such that $U_s(t) = U_0 = \text{const}$. In this way, the dynamics of this active Brownian particle, subject to passive-translational and active-rotational noises, is determined by its position $\boldsymbol{x}(t)$ and its direction of motion $\hat{\boldsymbol{u}}(t)$, computed from $\varphi(t)$, that obey the following Langevin equations:

$$\frac{d}{dt}\boldsymbol{x}(t) = U_0\,\hat{\boldsymbol{u}}(t) + \boldsymbol{\xi}_T(t), \tag{1a}$$

$$\frac{d}{dt}\varphi(t) = \xi_R(t). \tag{1b}$$

In this way, the temporal evolution of the particle's position [Eq. (1a)] is thus determined by two independent stochastic effects, one that corresponds to translational fluctuations due to the environmental noise and the other to the swimmer's velocity whose orientation is subject to active fluctuations [Eq. (1b)]. These same equations have been considered widely, particularly in Ref. [34], to model the motion of spherical platinum-silica Janus particles in a solution of water and H_2O_2.

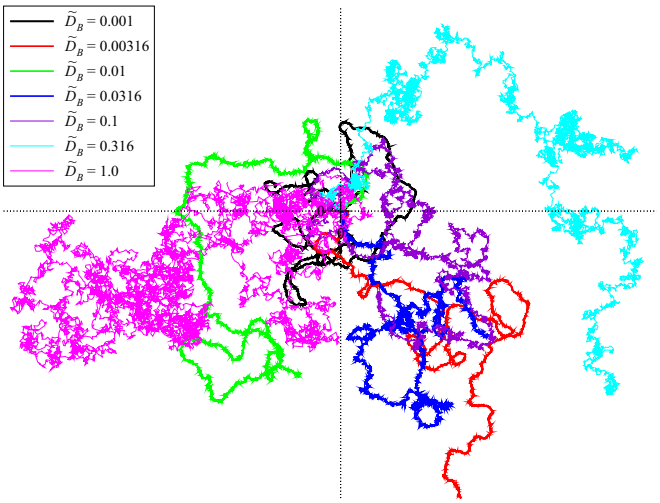

FIG. 1. (Color online) Single-particle trajectories for different values of $\widetilde{D}_B$, specifically 0.001, 0.00316, 0.01, 0.0316, 0.1, 0.316, and 1.0. Data are generated by solving Eq. (1) during 10^4 time steps; the initial position is chosen at the origin while the initial orientation is drawn from a uniform distribution in $[0,2\pi)$.

From now onward, we use D_Ω^{-1} and $U_0D_\Omega^{-1}$ as time and length scales, respectively, such that $\widetilde{D}_B \equiv D_BD_\Omega/U_0^2$ is the only free, dimensionless parameter of our analysis which coincides with the inverse of the so-called Péclet number, which in this case corresponds to the ratio of the advective transport coefficient, U_0^2/D_Ω, to the translational diffusion transport coefficient, D_B. For the Janus particles studied by Pallaci *et al.* in Ref. [27], we have that $D_\Omega^{-1} \approx 0.9\ \text{s}^{-1}$, $D_B \approx 0.34\ \mu\text{m}^2/\text{s}$ with swimming speeds between 0.3 and 3.3 μm/s. These values give $\widetilde{D}_B$ between 0.035 and 4.2. Numerical results, on the other hand, are obtained by integrating Eqs. (1) by use of the semi-implicit Euler or Euler-Cromer scheme, which improves on the standard Euler method. A time step of 0.005 was used in simulations. In Fig. 1 seven single-particle trajectories are presented to show the effect of varying $\widetilde{D}_B$; it can be noticed that the effects of persistence are conspicuous for small values of $\widetilde{D}_B$ (less-wiggly trajectories in Fig. 1, shown in thick lines).

An equation for the one-particle probability density $P(\boldsymbol{x},\varphi,t) \equiv \langle \delta(\boldsymbol{x}-\boldsymbol{x}(t))\delta(\varphi-\varphi(t))\rangle$ can be derived by differentiating this $P(\boldsymbol{x},\varphi,t)$ with respect to time, namely

$$\begin{aligned}\frac{\partial}{\partial t}P(\boldsymbol{x},\varphi,t) + U_0\hat{\boldsymbol{u}}\cdot\nabla P(\boldsymbol{x},\varphi,t) \\ = -\frac{\partial}{\partial\varphi}\langle\xi_R(t)\delta[\boldsymbol{x}-\boldsymbol{x}(t)]\delta[\varphi-\varphi(t)]\rangle \\ -\nabla\cdot\langle\boldsymbol{\xi}_T(t)\delta[\boldsymbol{x}-\boldsymbol{x}(t)]\delta[\varphi-\varphi(t)]\rangle,\end{aligned} \tag{2}$$

where $\langle\cdot\rangle$ denotes the average over-translational and rotational noise realizations, $\nabla = (\partial/\partial x, \partial/\partial y)$ and $\hat{\boldsymbol{u}} = (\cos\varphi, \sin\varphi)$.

The last two terms of Eq. (2) can be calculated by the use of Novikov's theorem [35,36], which states that for a functional $F[\beta(t)]$ of the stochastic Gaussian process

$\beta(t)$ with vanishing average, $\langle\beta(t)\rangle = 0$, and autocorrelation function, $\langle\beta(t)\beta(s)\rangle = 2\gamma\delta(t-s)$, γ being the noise intensity, the quantity $\langle\beta(t)F[\beta(t)]\rangle$ equals $\gamma\langle\widetilde{\delta}F[\beta(t)]/\widetilde{\delta}\beta(t)\rangle$, where $\widetilde{\delta}F/\widetilde{\delta}\beta$ denotes the variational derivative of F with respect to β. In the particular case of Eq. (2), $F[\xi_R(t)]$ and $F[\boldsymbol{\xi}_T(t)]$ correspond respectively to $\delta[\boldsymbol{x}-\boldsymbol{x}(t)]$ and $\delta[\varphi-\varphi(t)]$, whose explicit dependence on the processes $\xi_R(t)$ and $\boldsymbol{\xi}_T(t)$ is revealed through integration of Eqs. (1). By the use of this theorem and after some algebraic steps, we obtain the following Fokker-Planck equation for an active Brownian particle:

$$\frac{\partial}{\partial t}P(\boldsymbol{x},\varphi,t) + U_0\,\hat{\boldsymbol{u}}\cdot\nabla P(\boldsymbol{x},\varphi,t) = D_B\nabla^2 P(\boldsymbol{x},\varphi,t) + D_\Omega\frac{\partial^2}{\partial\varphi^2}P(\boldsymbol{x},\varphi,t). \tag{3}$$

We now start to analytically solve Eq. (3) with the initial condition $P(\boldsymbol{x},\varphi,0) = \delta^{(2)}(\boldsymbol{x})/2\pi$, which corresponds to the case when the particle departs from the origin in a random direction of motion drawn from a uniform distribution in $[-\pi,\pi]$, with $\delta^{(2)}(\boldsymbol{x})$ being the two-dimensional Dirac's δ function. To do so, we apply the Fourier transform to Eq. (3), and we obtain

$$\frac{\partial}{\partial t}\widetilde{P}(\boldsymbol{k},\varphi,t) + iU_0\,\hat{\boldsymbol{u}}\cdot\boldsymbol{k}\,\widetilde{P}(\boldsymbol{k},\varphi,t) = -D_B\boldsymbol{k}^2\widetilde{P}(\boldsymbol{k},\varphi,t) + D_\Omega\frac{\partial^2}{\partial\varphi^2}\widetilde{P}(\boldsymbol{k},\varphi,t), \tag{4}$$

where

$$\widetilde{P}(\boldsymbol{k},\varphi,t) = (2\pi)^{-1}\int d^2\boldsymbol{x}\,e^{-i\boldsymbol{k}\cdot\boldsymbol{x}}\,P(\boldsymbol{x},\varphi,t), \tag{5}$$

and $\boldsymbol{k} = (k_x,k_y)$ denotes the Fourier wave vector. For $U_0 = 0$, Eq. (4) has as solution the set of eigenfunctions $\{e^{-(D_Bk^2+D_\Omega n^2)t}e^{in\varphi}\}$ with n an integer. Thus we expand $\widetilde{P}(\boldsymbol{k},\varphi,t)$ on this set, expressly

$$\widetilde{P}(\boldsymbol{k},\varphi,t) = \frac{1}{2\pi}\sum_{n=-\infty}^{\infty}\widetilde{p}_n(\boldsymbol{k},t)e^{-(D_Bk^2+D_\Omega n^2)t}e^{in\varphi}, \tag{6}$$

with $k = |\boldsymbol{k}|$. This expansion features two advantages: On the one hand, it allows us to separate the effects of translational diffusion contained in the prefactor $e^{-D_Bk^2t}$ from the effects of rotational diffusion due to active fluctuations, as has been experimentally shown to occur for Janus particles driven by the local demixing of a binary chemical mixture due to local heating with light [37]. On the other, it enables the identification of the time scales associated to each Fourier mode n, whereby the higher the mode the faster it decays with time. In fact, one should expect in the asymptotic limit, when high modes have been damped out, a rotationally symmetric distribution. Additionally, notice that expansion (6) corresponds to the power series in $\hat{\boldsymbol{u}}$ of $\widetilde{P}(\boldsymbol{k},\varphi,t)$ [38,39] if the coefficients $\widetilde{p}_0,\widetilde{p}_{\pm1},\widetilde{p}_{\pm2},\ldots$, are identified with the entries of the respective rank 0, 1, 2, ..., tensors of such series (see the Appendix).

The coefficients of the expansion (6) are obtained by the use of the standard orthogonality relation among the Fourier basis functions $\{e^{in\varphi}\}$, explicitly

$$\widetilde{p}_n(\boldsymbol{k},t) = e^{(D_Bk^2+D_\Omega n^2)t}\int_{-\pi}^{\pi}d\varphi\;\widetilde{P}(\boldsymbol{k},\varphi,t)e^{-in\varphi}. \tag{7}$$

After substitution of Eq. (6) into Eq. (4) and use of the orthogonality of the Fourier basis functions we get the following set of coupled ordinary differential equations for the n-th coefficient of the expansion $\widetilde{p}_n(\boldsymbol{k},t)$, namely

$$\frac{d}{dt}\widetilde{p}_n = -\frac{U_0}{2}ik\,e^{-D_\Omega t}[e^{2nD_\Omega t}e^{-i\theta}\,\widetilde{p}_{n-1} + e^{-2nD_\Omega t}e^{i\theta}\,\widetilde{p}_{n+1}]. \tag{8}$$

Note that we have introduced the quantities $k_x \pm ik_y = ke^{\pm i\theta}$.

Our main interest lies on the coarse-grained p.d.f. $P_0(\boldsymbol{x},t) = \int_0^{2\pi}d\varphi\;P(\boldsymbol{x},\varphi,t)$, which gives the probability density of finding a particle at position $\boldsymbol{x}$ at time t independently of its direction of motion. This is given by the inverse Fourier transform of

$$\widetilde{P}_0(\boldsymbol{k},t) = e^{-D_Bk^2t}\widetilde{p}_0(\boldsymbol{k},t), \tag{9}$$

as can be checked from Eq. (7), $e^{-D_Bk^2t}$ being the translational diffusion propagator. Thereby, $P_0(\boldsymbol{x},t)$ is given by the convolution of the translational propagator with the probability distribution that retains the effects of the active rotational diffusion, $p_0(\boldsymbol{x},t)$, i.e.,

$$P_0(\boldsymbol{x},t) = \int d^2\boldsymbol{x}'G(\boldsymbol{x}-\boldsymbol{x}',t)p_0(\boldsymbol{x}',t), \tag{10}$$

with $p_0(\boldsymbol{x},t)$ the inverse Fourier transform of $\widetilde{p}_0(\boldsymbol{k},t)$ and where

$$G(\boldsymbol{x},t) = \frac{e^{-\boldsymbol{x}^2/4D_Bt}}{4\pi D_Bt} \tag{11}$$

is the Gaussian propagator of translational diffusion in two dimensions.

In principle $\widetilde{p}_0(\boldsymbol{k},t)$ can be found by solving the infinite set of coupled ordinary differential equations (8), with the initial conditions $\widetilde{p}_n(\boldsymbol{k},0) = \delta_{n,0}/2\pi$, a task that is practically unattainable. Notwithstanding this, we use the explicit appearance of the time scales in the factor $e^{-D_\Omega n^2t}$ associated to each mode n in the expansion (6) to approach the solution from the diffusive limit. Thus, if we consider up to modes $n\pm2$, Eqs. (8) reduce to

$$\frac{d}{dt}\widetilde{p}_0 = -\frac{U_0}{2}ik\,e^{-D_\Omega t}[e^{-i\theta}\,\widetilde{p}_{-1} + e^{i\theta}\,\widetilde{p}_1], \tag{12a}$$

$$\frac{d}{dt}\widetilde{p}_{\pm1} = -\frac{U_0}{2}ik\,[e^{D_\Omega t}e^{\mp i\theta}\,\widetilde{p}_0 + e^{-3D_\Omega t}e^{\pm i\theta}\,\widetilde{p}_{\pm2}], \tag{12b}$$

$$\frac{d}{dt}\widetilde{p}_{\pm2} = -\frac{U_0}{2}ik\,[e^{3D_\Omega t}e^{\mp i\theta}\,\widetilde{p}_{\pm1}], \tag{12c}$$

whereby, after some algebra, Eqs. (12a) and (12b) are combined into a single equation for $\widetilde{p}_0$, that is,

$$\frac{d^2}{dt^2}\widetilde{p}_0 + D_\Omega\frac{d}{dt}\widetilde{p}_0 = -\frac{U_0^2}{2}k^2\widetilde{p}_0 - \frac{U_0^2}{4}k^2e^{-4D_\Omega t}(e^{2i\theta}\,\widetilde{p}_2 + e^{-2i\theta}\,\widetilde{p}_{-2}). \tag{13}$$

As is shown in the Appendix, Eq. (13) corresponds to the diffusion-drift approximation used in the hydrodynamic treatment in Refs. [38,39].

A. The diffusive limit

At this stage we argue that in the diffusive limit we may neglect the second term in the right-hand side of Eq. (13) (the contribution of high harmonics modes decay so fast that only the first modes $n = 0, \pm 1$ would be enough for an approximated description of rotationally symmetric solution) this approximation leads to the telegrapher's equation [40,41]

$$\frac{d^2}{dt^2}\widetilde{p}_0 + D_\Omega \frac{d}{dt}\widetilde{p}_0 = -\frac{U_0^2}{2}k^2\widetilde{p}_0, \tag{14}$$

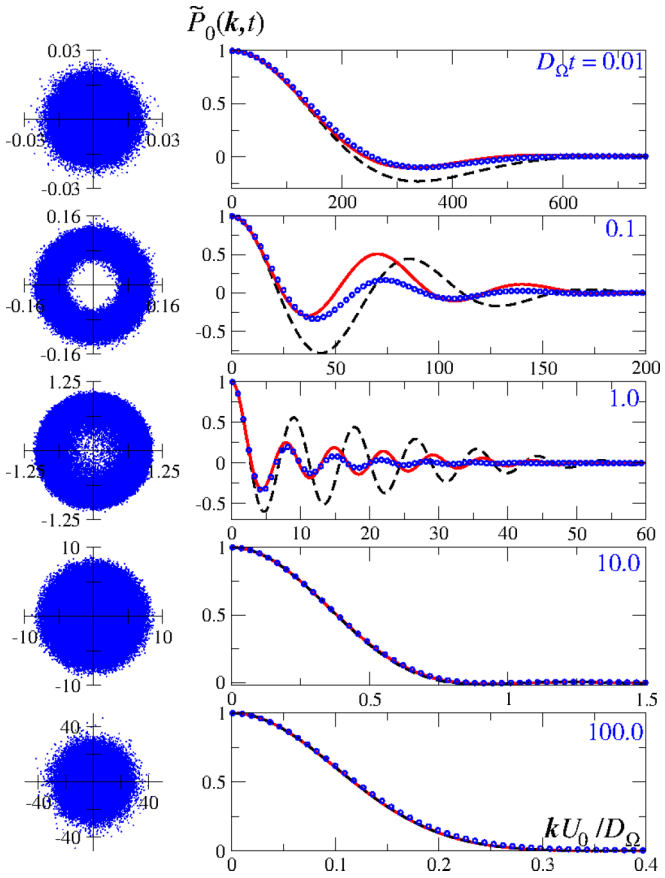

FIG. 2. (Color online) Left: Snapshots of the positions of 10^5 particles taken at different times, namely, from top to bottom, $D_\Omega t = 0.01, 0.1, 1.0, 10$, and 100, for an inverse Péclet number $\widetilde{D}_B = 0.001$. Notice the formation of a rotationally symmetric ringlike structure (second panel from top) that develops from a Gaussian distribution due to the effects of persistence in the motion of the particles. The structure fades out as time passes (third and fourth images from top) to reach a Gaussian distribution at long times (bottom image). Right: Dimensionless p.d.f. $\widetilde{P}_0(\boldsymbol{k},t)$ are shown as function of kU_0/D_Ω. The black-dashed lines correspond to the solutions obtained from (16), the solid red ones correspond to the solutions obtained from inversion of the Laplace transform of (23), and the blue circles give the exact p.d.f. obtained from the numerical Fourier transform of the data shown in the left column.

which is rotationally symmetric in the $\boldsymbol{k}$ space and, therefore, gives rise to rotationally symmetric solutions in spatial coordinates if initial conditions with the same symmetry are chosen. One may check that Eq. (14) has the solution

$$\widetilde{p}_0(\boldsymbol{k},t) = \widetilde{p}_0(\boldsymbol{k},0)\, e^{-D_\Omega t/2}\left[\frac{D_\Omega}{2\omega_k}\sin\omega_k t + \cos\omega_k t\right], \tag{15}$$

with $\omega_k^2 \equiv U_0^2k^2/2 - D_\Omega^2/4$. From this expression $\widetilde{P}_0(\boldsymbol{k},t)$ follows straightforwardly

$$\widetilde{P}_0(\boldsymbol{k},t) = \frac{1}{2\pi}\, e^{-(D_B k^2 + D_\Omega/2)t}\left[\frac{D_\Omega}{2\omega_k}\sin\omega_k t + \cos\omega_k t\right]. \tag{16}$$

This solution is shown as a function of kU_0/D_Ω at different times in Fig. 2 (black dashed line).

In the asymptotic limit ($t \to \infty$), at which the coherent wavelike behavior related to the second-order time derivative in Eq. (14) can be neglected (mainly due to the random dispersion of the particles direction of motion), $p_0(\boldsymbol{x},t)$ tends to a Gaussian distribution with diffusion constant $U_0^2/2D_\Omega$, namely

$$p_0(\boldsymbol{x},t) \underset{t\to\infty}{\longrightarrow} \frac{e^{-\boldsymbol{x}^2/4(U_0^2/2D_\Omega)t}}{4\pi\left(U_0^2/2D_\Omega\right)t}. \tag{17}$$

Substitution of this last expression into Eq. (10) and performing the integral, one gets in the long-time regime

$$P_0(\boldsymbol{x},t) = \frac{e^{-\boldsymbol{x}^2/4\left(D_B + U_0^2/2D_\Omega\right)t}}{4\pi\left(D_B + U_0^2/2D_\Omega\right)t}, \tag{18}$$

from which the classical effective diffusion constant $D = D_B + U_0^2/2D_\Omega$ is deduced [27].

In the short-time regime $D_\Omega t \ll 1$, we approximate $\widetilde{p}_0(\boldsymbol{k},t) \approx \widetilde{p}_0(\boldsymbol{k},0) = (2\pi)^{-1}$ and the p.d.f. in spatial coordinates corresponds to the Gaussian

$$P_0(\boldsymbol{x},t) \approx \frac{1}{2\pi}\frac{e^{-\boldsymbol{x}^2/4D_B t}}{4\pi D_B t}. \tag{19}$$

Though it is a difficult task to obtain from Eq. (10) the explicit dependence on $\boldsymbol{x}$ and t of P_0, a formula in terms of a series expansion of the operator ∇^2 applied to $G(\boldsymbol{x},t)$ can be derived to say

$$P_0(\boldsymbol{x},t) = \frac{1}{2\pi}e^{-D_\Omega t/2}\sum_{s=0}^{\infty}\frac{1}{(2s)!}\left(1 + \frac{D_\Omega t}{2}\frac{1}{2s+1}\right) \times \left(\frac{D_\Omega t}{2}\right)^{2s}\left(1 - \frac{2U_0^2}{D_\Omega^2}\nabla^2\right)^s G(\boldsymbol{x},t). \tag{20}$$

Note that the last formula can be rewritten in terms of ∂_t instead of ∇^2 by using that $\nabla^2 G = D_B^{-1}\partial_t G$.

B. A shorter time description: Memory effects

If Eq. (13) is considered along (12c), we obtain after some algebra that

$$\frac{d^2}{dt^2}\widetilde{p}_0 + D_\Omega\frac{d}{dt}\widetilde{p}_0 = -U_0^2k^2\int_0^t ds\,\eta(t-s)\widetilde{p}_0(\boldsymbol{k},s) - \frac{U_0^2}{4}e^{-4D_\Omega t}\widetilde{q}(\boldsymbol{k}), \tag{21}$$

where $\eta(t) = (3/4)\,\delta(t) - D_\Omega e^{-4D_\Omega t}$ is a memory function that takes into account the Fourier modes $\widetilde{p}_{\pm 2}$ and $\widetilde{q}(\boldsymbol{k})$ is a term that depends only on the initial conditions (to be specific) $\widetilde{q}(\boldsymbol{k}) = k^2[e^{i2\theta}\widetilde{p}_2(\boldsymbol{k},0) + e^{-i2\theta}\widetilde{p}_{-2}(\boldsymbol{k},0) - \widetilde{p}_0(\boldsymbol{k},t)]$. This last term reduces to $-k^2/2\pi$ for the initial conditions considered in our analysis.

The solution to Eq. (21) can be found by use of the Laplace transform, and explicitly we get

$$\widetilde{p}_0(\boldsymbol{k},\epsilon) = \frac{(\epsilon + 4D_\Omega)(\epsilon + D_\Omega) + U_0^2k^2/4}{(\epsilon + 4D_\Omega)\left[\epsilon^2 + D_\Omega\epsilon + (3/4)U_0^2k^2\right] - U_0^2D_\Omega k^2}. \tag{22}$$

From this last expression, $\widetilde{P}_0(\boldsymbol{k},\epsilon)$ can be found by use of the frequency shifting property of the Laplace transform, thus

$$\widetilde{P}_0(\boldsymbol{k},\epsilon) = \widetilde{p}_0(\boldsymbol{k},\epsilon + D_Bk^2). \tag{23}$$

Inversion of the Laplace transform of (23) evaluated at times $D_\Omega t = 0.01$ 0.1, 1.0 10.0, and 100.0 is shown as function of kU_0/D_Ω in Fig. 2 (red solid line).

In Fig. 2, snapshots of the positions of 10^5 particles (left column) obtained from numerical simulations with an inverse Péclet number $\widetilde{D}_B = 0.001$, taken at the times $D_\Omega t = 0.01, 0.1,$ 1.0, 10, and 100, are shown. The plots in the right column show $P_0(\boldsymbol{k},t)$ as a function of kU_0/D_Ω at the corresponding time values to those in the left column. The black dashed and red solid lines correspond to (16) and (23), respectively, while the blue circles represent the exact p.d.f. obtained from the Fourier transform of the data obtained from the simulation shown in the left column. The first pair of images from the top ($D_\Omega t = 0.01$), correspond to a p.d.f. that has departed from the Gaussian given by Eq. (19); notice the good agreement of the solution obtained from (23) with the exact result. At $D_\Omega t = 0.1$ (second pair of images from top), the formation of a rotationally symmetric ringlike structure, due to the persistence effects on the particles' motion, is observed. It is at this regime where both solutions built from (15) and (22) depart from the exact result; this indicates that a framework that goes beyond the "drift diffusion" approximation that takes into account higher Fourier modes is necessary. Subsequently, the structure starts to fade out (third pair of images from top) and while the solution (16) is not valid at this time, the solution obtained from (23) becomes a much better approximation. For longer times (fourth and fifth pair of images from the top) the solutions start turning into the Gaussian distribution [Eq. (18)], where both solutions are in good agreement with the exact solution.

It is clear that the deviation of the solutions (16) and (23) from the exact result, in the time regime $D_\Omega t \lesssim 1$, originates in the prominent persistence effects of motion which are not accurately captured by the approximations made to obtain Eqs. (14) and (21), respectively. In such a time regime, our approximations inherently contain a wake effect that is characteristic of the solution of the two-dimensional wave equation [9]. Notwithstanding this and as is shown later, the mean-square displacement computed from our first approximation and the kurtosis computed from the second one coincide with the exact ones computed from numerical simulations at all time regimes.

III. MEAN-SQUARE DISPLACEMENT

What the effects of self-propulsion are on the diffusive behavior of the system is a question that has been addressed in several experimental and theoretical studies, and the msd, being a measure of the covered space as a function of time by the random particle, has been of physical relevance in both contexts. Indeed, the msd is obtained in many experimental situations that consider active particles [18,34,42]; hence it is a way of validating existing theoretical approaches. On the other hand, it is known that the diffusion coefficient of active particles depends on the particle density, due mainly to excluded volume effects of the particles. Here we assume a system that is diluted enough to neglect those effects.

In what follows, an exact analytical expression for the msd is obtained. First notice that after the application of the operator $-\nabla_{\boldsymbol{k}}^2$ to $\widetilde{P}_0(\boldsymbol{k},t) = e^{-D_Bk^2t}\widetilde{p}_0(\boldsymbol{k},t)$, evaluation at $\boldsymbol{k} = 0$ results in $\langle \boldsymbol{x}^2(t)\rangle = 4D_Bt + \langle \boldsymbol{x}^2(t)\rangle_0$, which leads straightforwardly to the pair of relations

$$\frac{d}{dt}\langle \boldsymbol{x}^2(t)\rangle = 4D_B + \frac{d}{dt}\langle \boldsymbol{x}^2(t)\rangle_0, \tag{24a}$$

$$\frac{d^2}{dt^2}\langle \boldsymbol{x}^2(t)\rangle = \frac{d^2}{dt^2}\langle \boldsymbol{x}^2(t)\rangle_0, \tag{24b}$$

where $\langle\cdot\rangle$, $\langle\cdot\rangle_0$ denote the average of $(\cdot)$ taken with $P_0(\boldsymbol{x},t)$ and $p_0(\boldsymbol{x},t)$ as the probability measure, respectively. The quantity $\frac{d^2}{dt^2}\langle \boldsymbol{x}^2(t)\rangle_0$ can be computed directly after applying $-\nabla_{\boldsymbol{k}}^2$ to Eq. (13) and evaluating at $\boldsymbol{k} = 0$, i.e.,

$$\begin{aligned}\frac{d^2}{dt^2}\langle \boldsymbol{x}^2(t)\rangle_0 + D_\Omega\frac{d}{dt}\langle \boldsymbol{x}^2(t)\rangle_0 &= \frac{U_0^2}{2}\left[\nabla_{\boldsymbol{k}}^2\left(k_x^2 + k_y^2\right)\widetilde{p}_0\right]_{\boldsymbol{k}=0} + \frac{U_0^2}{4}e^{-4D_\Omega t}\\ &\quad\times\left\{\nabla_{\boldsymbol{k}}^2[(k_x - ik_y)^2\widetilde{p}_{-2} + (k_x + ik_y)^2\widetilde{p}_2]\right\}_{\boldsymbol{k}=0}.\end{aligned} \tag{25}$$

It is easy to show that the first term of the right-hand side of the last equation is $2U_0^2$ while the next term, which involves the modes $\widetilde{p}_{\pm 2}$, vanishes identically, and thus we get

$$\frac{d^2}{dt^2}\langle \boldsymbol{x}^2(t)\rangle_0 + D_\Omega\frac{d}{dt}\langle \boldsymbol{x}^2(t)\rangle_0 = 2U_0^2. \tag{26}$$

Notice that the same result could be obtained from the telegrapher Eq. (14) after multiplying it by $\boldsymbol{x}^2$ and integrating over the whole space. With the use of Eqs. (24) we finally have that

$$\frac{d^2}{dt^2}\langle \boldsymbol{x}^2(t)\rangle + D_\Omega\frac{d}{dt}\langle \boldsymbol{x}^2(t)\rangle = 2U_0^2 + 4D_BD_\Omega, \tag{27}$$

whose solution can be easily found, namely

$$\langle \boldsymbol{x}^2(t)\rangle = 4\frac{U_0^2}{D_\Omega^2}\left[\left(\widetilde{D}_B + \frac{1}{2}\right)D_\Omega t - \frac{1}{2}(1 - e^{-D_\Omega t})\right], \tag{28}$$

where we have used that $(d/dt)\,\langle \boldsymbol{x}^2(t)\rangle\big|_{t=0} = 4D_B$ in this case.

The linear dependence on time of the msd, expected in the Gaussian regime, is checked straightforwardly from Eq. (28).

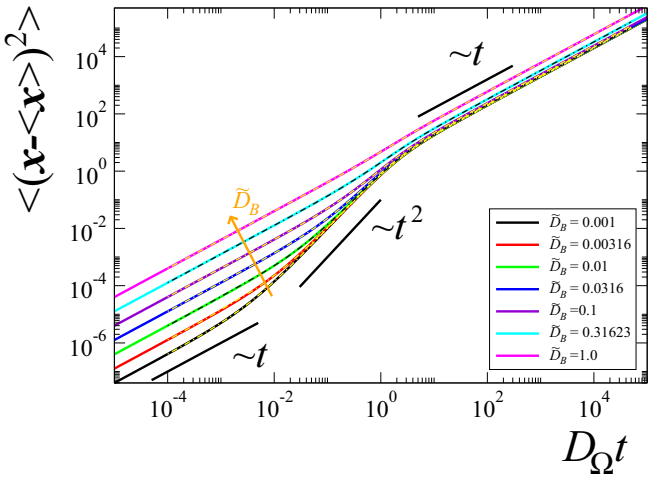

FIG. 3. (Color online) Mean-square displacement in units of U_0^2/D_Ω^2 as function of the dimensionless time $D_\Omega t$ for different values of the inverse Péclet number $\widetilde{D}_B$, namely 0.001, 0.0031, 0.01, 0.0316, 0.1, 0.3162, and 1.0. Solid lines correspond to the analytical expression given by Eq. (28), while the thin, dash-dotted lines correspond to the results obtained from numerical simulations (see text) solving Eqs. (1a) and (1b).

In the long-time regime we get

$$\langle \boldsymbol{x}^2(t)\rangle \xrightarrow[D_\Omega t\to\infty]{} 4\left(D_B + \frac{U_0^2}{2D_\Omega}\right)t, \tag{29}$$

which is a classical result indicating that the effective diffusion of a self-propelled particle is enhanced by its activity [3]. In the opposite limit, we find

$$\langle \boldsymbol{x}^2(t)\rangle \xrightarrow[D_\Omega t\to 0]{} 4D_B t + \left(2D_B D_\Omega + U_0^2\right)t^2, \tag{30}$$

which shows the quadratic correction due to persistence to the standard linear behavior with diffusion constant D_B. Notice that the coefficient of t^2 can be interpreted as the effective swimming speed $U_e = \sqrt{2D_B D_\Omega + U_0^2}$, which has been extracted from the msd data fit in experiments of active Janus particles in hydrogen peroxide [5] and self-thermophoretic Janus particles in laser beams [43].

In order to validate our theoretical findings, we have also performed Brownian dynamics simulations implemented to solve Eqs. (1a) and (1b). Figure 3 shows a comparison among our theoretical prediction for any time given by Eq. (28) (solid lines) and our Brownian dynamics simulations (dashed lines) that take into account averages over an ensemble of 10^5 trajectories. We observe an excellent agreement among theory and Brownian simulations for each value chosen of $\widetilde{D}_B$ (each plotted line corresponds to a different value of $\widetilde{D}_B$). Additionally, Fig. 3 also indicates that the crossover from a linear behavior to a quadratic one tends to disappear for values of $\widetilde{D}_B$ around 1, for which translational diffusion dominates over the effects of the rotational one. The absence of a transition from a linear to a quadratic behavior has also been reported by ten Hagen *et al.* [18]. They suggest that the interplay between different choices of initial orientations and of persistence times, is the key ingredient for the appearance of the crossover in the msd.

IV. KURTOSIS

Once we have obtained approximately $P_0(\boldsymbol{x},t)$ from Eq. (3), we wish to characterize its departure from a Gaussian p.d.f. as a function of time. Indeed, non-Gaussianity has been a relevant topic in the study of transport properties in different systems, and hence its analysis in systems of active particle is relevant from the point of view of statistical mechanics. To this purpose, we calculate the kurtosis κ of $P_0(\boldsymbol{x},t)$, which for our convenience is given explicitly by [44]

$$\kappa = \langle[(\boldsymbol{x}-\langle\boldsymbol{x}\rangle)^T\Sigma^{-1}(\boldsymbol{x}-\langle\boldsymbol{x}\rangle)]^2\rangle, \tag{31}$$

where $\boldsymbol{x}^T$ denotes the transpose of the vector $\boldsymbol{x}$ and Σ is the 2×2 matrix defined by the average of the dyadic product $(\boldsymbol{x}-\langle\boldsymbol{x}\rangle)^T\cdot(\boldsymbol{x}-\langle\boldsymbol{x}\rangle)$. In addition, it can be shown that for circularly symmetric distributions, as the ones considered in the present study, Eq. (31) reduces to

$$\kappa = 4\frac{\langle \boldsymbol{x}^4(t)\rangle_r}{\langle \boldsymbol{x}^2(t)\rangle_r^2}, \tag{32}$$

where $\langle\cdot\rangle_r$ denotes the radial average over the radial probability density distribution, namely $\langle\cdot\rangle_{\rm rad} = \int_0^\infty dr\, r P(r)(\cdot)$.

As we can see, Eq. (32) requires the calculation of the fourth moment $\langle \boldsymbol{x}^4(t)\rangle_r$ that can be obtained, in the Laplacian domain, from Eq. (23) through the prescription

$$\widetilde{\langle \boldsymbol{x}^4(\epsilon)\rangle_r} = \left(\frac{1}{k}\frac{\partial}{\partial k}k\frac{\partial}{\partial k}\right)^2 \widetilde{P}_0(\boldsymbol{k},\epsilon)\big|_{k=0}. \tag{33}$$

One can verify from Eq. (13) that the modes $\widetilde{p}_{\pm 2}$ do contribute to the fourth-moment of $\widetilde{p}_0(\boldsymbol{k},t)$ and therefore the Telegrapher equation (14) only gives a crude approximation for the fourth-moment.

After straightforward algebraic steps, we explicitly find that the fourth-moment is given by

$$\widetilde{\langle \boldsymbol{x}^4(\epsilon)\rangle_r} = \frac{8D_B^2}{\epsilon^3}\left[1 + \frac{4U_0^2}{D_B}\frac{(3\epsilon+2D_\Omega)}{(\epsilon+D_\Omega)^2} + \frac{U_0^4}{D_B^2}\frac{(3\epsilon+8D_\Omega)}{(\epsilon+D_\Omega)^2(\epsilon+4D_\Omega)}\right], \tag{34}$$

and after the application of the inverse Laplace transform we get the explicit time dependence

$$\langle \boldsymbol{x}^4(t)\rangle_r = 2^5\frac{U_0^4}{D_\Omega^4}\left[(D_\Omega t)^2\left(\widetilde{D}_B+\frac{1}{2}\right)^2 - \widetilde{D}_B\, D_\Omega t(1-e^{-D_\Omega t})\right] + \frac{U_0^4}{D_\Omega^4}\left[\frac{87}{2} - 30D_\Omega t\left(1+\frac{4}{9}e^{-D_\Omega t}\right) - \frac{49}{9}e^{-D_\Omega t} + \frac{1}{144}e^{-4D_\Omega t}\right]. \tag{35}$$

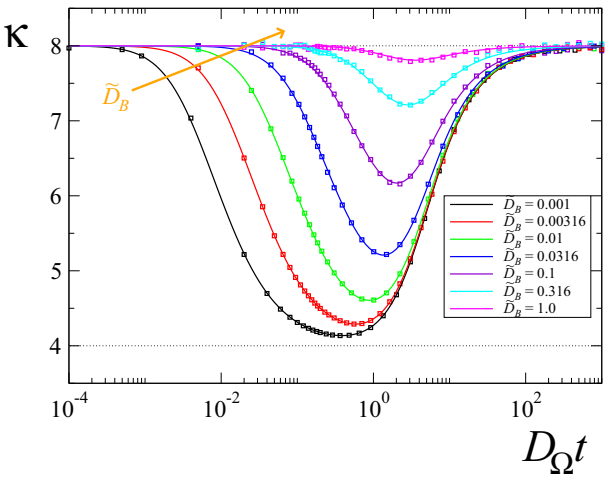

FIG. 4. (Color online) Kurtosis of the particles distribution as function of the dimensionless time $D_\Omega t$ for different values of $\widetilde{D}_B$, namely 0.001, 0.0031, 0.01, 0.0316, 0.1, 0.3162, and 1.0. Solid lines correspond to the exact analytical expression given by the quotient of Eq. (35) and the square of Eq. (28), while the symbols mark the values of the kurtosis obtained from numerically solving Eqs. (1a) and (1b). Thin-dotted lines mark the values 8 and 4 that correspond, respectively, in two dimensions, to a Gaussian distribution and a ringlike distribution [9].

The latter analytical expression is used in Fig. 4 to plot the kurtosis, specifically, the ratio of Eq. (35) to the square of Eq. (28). In that figure, kurtosis is plotted as a function of the dimensionless time $D_\Omega t$ for different values of $\widetilde{D}_B$ (solid lines), while the corresponding exact results from Brownian dynamics that solve Eqs. (1a) and (1b) are shown in symbols. Notice that our theoretical calculations for different values of $\widetilde{D}_B$ capture qualitatively the results obtained from experimental data of self-propelled Janus particles in different concentrations of hydrogen peroxide solutions [34].

We observe that the kurtosis shows a clear nonmonotonic behavior for $\widetilde{D}_B \lesssim 1$, namely it starts to diminish from $\kappa = 8$ as

$$\kappa \simeq 8\left[1 - \left(\frac{D_\Omega t}{2\widetilde{D}_B}\right)^2\right] \tag{36}$$

until it reaches a minimum that depends on the inverse of the Péclet number $\widetilde{D}_B$ at a time around D_Ω^{-1}. This behavior has been observed in experiments with Janus particles in three dimensions [34] and theoretically predicted in one quasi-one-dimensional channels [45] and becomes less and less evident as the translational diffusion coefficient surpasses the effective diffusion coefficient that originates in the rotational diffusion, U_0^2/D_Ω. In the limit of vanishing translational diffusion, the kurtosis is a monotonic increasing function of time, with $\kappa = 4$ as its minimum value [9].

On the other hand, the persistence effects induced by orientational correlations are revealed in the diminishing regime of the kurtosis, as is shown in Fig. 4 for the cases in which $\widetilde{D}_B \lesssim 1$ (see Table I for the values of κ corresponding to the snapshots shown on the left column of Fig. 2). In this regime the orientational correlations surpass the effects of translational noise hence allowing the particles to move

TABLE I. Kurtosis values at the times $D_\Omega t$ that are close to those values chosen to generate the data shown in the left column of Fig. 2 ($\widetilde{D}_B = 0.001$).

$D_\Omega t$	0.01	0.1	1.01	10.245	100.08
κ	5.9598	4.3111	4.2729	6.7621	7.8713

persistently outwardly from the origin and giving rise to circularly symmetric, ringlike distributions as the one shown at left in Fig. 2 (second from top) at $D_\Omega t = 0.1$ for $\widetilde{D}_B = 0.001$. Afterwards, this ringlike distribution turns into a Gaussian distribution as the orientational correlations die out.

At later times the kurtosis starts to increase as

$$\kappa \simeq 8\left[1 - \frac{\widetilde{D}_B + \frac{15}{16}}{\left(\widetilde{D}_B + \frac{1}{2}\right)^2}(D_\Omega t)^{-1}\right], \tag{37}$$

reaching the value 8 in the asymptotic limit. Once again, Eq. (37) shows that kurtosis has a Gaussian behavior for long times. This result has also been validated using Brownian dynamics and is shown in Fig. 4, where for long values of the dimensionless time, κ tends again to a value of 8.

V. FINAL COMMENTS AND CONCLUSIONS

We have presented an analysis for the coarse-grained probability density distribution of finding a self-propelled particle at position $\boldsymbol{x}$ at time t regardless of its direction of motion. This distribution is directly connected with the marginal distribution in one dimension, which is acquired from experimental measurements, in systems of Janus particles in H_2O-H_2O_2 solutions [34]. To be precise, the inverse of the Péclet number $\widetilde{D}_B$ in our study can be translated into the hydrogen peroxide concentration through the particle swimming speed, whose dependence on H_2O_2 concentration is measured. For moderately small values of $\widetilde{D}_B$, i.e., $\widetilde{D}_B \sim 0.1$, the effects of persistence of active motion are not important and the situation corresponds to the case of low hydrogen peroxide concentrations ($\sim$5%) experiments in Ref. [34]. For 10–15% concentrations, which correspond to smaller values of $\widetilde{D}_B$, the distribution of particles in one directions shows a characteristic double peak (see Fig. 7 of Ref. [34]), which corresponds to the projection of the ringlike distribution shown in Fig. 2, in one direction.

In addition, the first moments of our calculated p.d.f., namely the mean-square displacement and the kurtosis, were obtained in an analytical and exact manner [Eqs. (28) and (35)]. The classical result of enhanced diffusion due to activity was recovered, Eq. (29). We want to point out that despite what Fig. 3 suggests, that is to say, that the long-time linear dependence of the msd, characteristic of normal diffusion, is reached at finite times $D_\Omega t \sim 1$, expression (37) shows that it slowly approaches such behavior as $(D_\Omega t)^{-1}$. This conclusion is reenforced by the fact that the msd (28) divided by the asymptotic limit (29) differs from 1 as $[2(\widetilde{D}_B + 1/2)D_\Omega t]^{-1}$. In contrast, in the short-time regime, the distribution departs with time from a Gaussian distribution as $8(D_\Omega t/2\widetilde{D}_B)^{-2}$.

In summary, we have found a method and obtained with it an analytical solution to the Smoluchowski equation of an

active Brownian particle self-propelling with constant velocity U_0. We used a Fourier approach and exploited the circular symmetry of the probability distribution function to obtain an infinite system of coupled ordinary differential equations for the coefficients of the Fourier series of the complete probability density. Our formalism showed that in order to have a whole description for the particles diffusion, given by the mean-squared displacement, only the lowest three Fourier coefficients of the expansion (5) suffice; however, the next two Fourier coefficients are needed to have the exact time dependence of the kurtosis. We also validated these findings by performing Brownian dynamics simulations that showed an excellent agreement among theory and simulations.

Future directions for this research would include developing a systematic method to analytically approach the solution of a Smoluchowski equation for confined active particles and/or particles interacting among them.

ACKNOWLEDGMENTS

F.J.S. acknowledges support from DGAPA-UNAM through Grant No. PAPIIT-IN113114. M.S. thanks CONACyT and Programa de Mejoramiento de Profesorado (PROMEP) for partially funding this work.

APPENDIX: CONNECTION WITH THE HYDRODYNAMIC DESCRIPTION

If the powers of $\cos\varphi$ and $\sin\varphi$ are gathered from the Fourier expansion given by Eq. (6), one can rewrite it as [38,39]

$$\widetilde{P}(\boldsymbol{k},\varphi,t) = e^{-D_B k^2 t}[\widetilde{\varrho}(\boldsymbol{k},t) + e^{-D_\Omega t}\widetilde{\boldsymbol{V}}(\boldsymbol{k},t)\cdot\hat{\boldsymbol{u}} + e^{-2D_\Omega t}\hat{\boldsymbol{u}}\cdot\widetilde{\mathbb{W}}(\boldsymbol{k},t)\cdot\hat{\boldsymbol{u}} + \cdots], \tag{A1}$$

with $\hat{\boldsymbol{u}} = (\cos\varphi, \sin\varphi)$. This power series in $\hat{\boldsymbol{u}}$ lets the Fourier transform of the hydrodynamic fields to be recognized in terms of the modes $\widetilde{p}_n$, namely the scalar (zero rank tensor) density field

$$\widetilde{\varrho}(\boldsymbol{k},t) = \frac{1}{2\pi}\widetilde{p}_0(\boldsymbol{k},t), \tag{A2}$$

the vectorial (first rank tensor) field $\widetilde{\boldsymbol{V}}(\boldsymbol{k},t)$ with components

$$\widetilde{V}_x(\boldsymbol{k},t) = \frac{1}{2\pi}\left[\widetilde{p}_{-1}(\boldsymbol{k},t) + \widetilde{p}_1(\boldsymbol{k},t)\right], \tag{A3a}$$

$$\widetilde{V}_y(\boldsymbol{k},t) = \frac{i}{2\pi}\left[\widetilde{p}_1(\boldsymbol{k},t) - \widetilde{p}_{-1}(\boldsymbol{k},t)\right], \tag{A3b}$$

the symmetric, traceless, second-rank tensorial field $\widetilde{\mathbb{W}}(\boldsymbol{k},t)$ with entries

$$\widetilde{\mathbb{W}}_{xx}(\boldsymbol{k},t) = -\widetilde{\mathbb{W}}_{yy}(\boldsymbol{k},t) = \frac{1}{2\pi}\left[\widetilde{p}_2(\boldsymbol{k},t) + \widetilde{p}_{-2}(\boldsymbol{k},t)\right], \tag{A4a}$$

$$\widetilde{\mathbb{W}}_{xy}(\boldsymbol{k},t) = \widetilde{\mathbb{W}}_{yx}(\boldsymbol{k},t) = \frac{i}{2\pi}\left[\widetilde{p}_2(\boldsymbol{k},t) - \widetilde{p}_{-2}(\boldsymbol{k},t)\right], \tag{A4b}$$

and so on. These quantities satisfy the equations

$$\frac{\partial}{\partial t}\widetilde{\varrho} + \frac{U_0}{2}e^{-D_\Omega t}\, i k_i \widetilde{V}_i = 0, \tag{A5a}$$

$$\frac{\partial}{\partial t}\widetilde{V}_i + U_0 e^{D_\Omega t}\, i k_i \widetilde{\varrho} + \frac{U_0}{2}e^{-D_\Omega t}\, i k_j \widetilde{\mathbb{W}}_{ij} = 0, \tag{A5b}$$

$$\frac{\partial}{\partial t}\widetilde{\mathbb{W}}_{xx} + \frac{U_0}{2}e^{D_\Omega t}\, i(k_x V_x - k_y V_y) + 2D_\Omega \widetilde{\mathbb{W}}_{xx} = 0, \tag{A5c}$$

$$\frac{\partial}{\partial t}\widetilde{\mathbb{W}}_{xy} + \frac{U_0}{2}e^{D_\Omega t}\, i(k_x V_y + k_y V_x) + 2D_\Omega \widetilde{\mathbb{W}}_{xy} = 0, \tag{A5d}$$

obtained by substitution of the series (A1) into Eq. (4), followed by integration over φ when multiplying the resulting equation by the scalar 1, the vector $\hat{\boldsymbol{u}}$, and the tensor $\hat{\boldsymbol{u}}\hat{\boldsymbol{u}}$, respectively. Einstein's convention must be understood when repeated indexes appear. Equations (A5) provide equivalent information as Eqs. (12), for example, Eq. (12a) corresponds to the continuity equation (A5a) for the probability distribution that carries out the information about the rotational part of motion, in spatial coordinates $\partial_t\varrho(\boldsymbol{x},t) + \nabla\cdot\boldsymbol{J}(\boldsymbol{x},t) = 0$, with $\boldsymbol{J}(\boldsymbol{x},t)$ the inverse Fourier transform of $\widetilde{\boldsymbol{J}}(\boldsymbol{k},t) = (U_0/2)e^{-D_\Omega t}\widetilde{\boldsymbol{V}}(\boldsymbol{k},t)$. Similarly, Eqs. (12b) and (12c) can be rewritten in the form (A5b) and (A5c)–(A5d), respectively.

The dynamics for $\widetilde{\boldsymbol{V}}$ depends explicitly on the dynamics of $\widetilde{\varrho}$ and of the components of $\widetilde{\mathbb{W}}$; these last ones relax due to rotational diffusion at the time scale $(2D_\Omega)^{-1}$ and are driven by fluxlike terms of $\widetilde{\boldsymbol{V}}$. After substitution of the explicit solution of Eqs. (A5c) and (A5d) in Eq. (A5b) we get

$$\frac{\partial}{\partial t}\widetilde{V}_i(\boldsymbol{k},t) + U_0 e^{D_\Omega t}\, i k_i\, \widetilde{\varrho}(\boldsymbol{k},t) + \frac{U_0^2}{4}k^2\int_0^t ds\, e^{-3D_\Omega(t-s)}\,\widetilde{V}_i(\boldsymbol{k},s) = 0, \tag{A6}$$

where the initial condition $\widetilde{\mathbb{W}}_{ij}(\boldsymbol{k},0) = 0$, derived from the initial conditions $\widetilde{P}(\boldsymbol{k},\varphi,0) = (2\pi)^{-2}$, has been used.

Solutions to (A5a) and (A6) can be obtained in a direct manner by the use of the Laplace transform, and such procedure leads, after some rearrangements, to

$$\widetilde{\varrho}(\boldsymbol{k},\epsilon) = \frac{\widetilde{\varrho}(\boldsymbol{k},0)}{\epsilon + \frac{U_0^2k^2/2}{\epsilon + D_\Omega + \frac{U_0^2k^2/4}{\epsilon+4D_\Omega}}}, \tag{A7}$$

which can be shown to coincide with expression (22) and to

$$\widetilde{V}_i(\boldsymbol{k},\epsilon) = \frac{-ik_iU_0}{\epsilon + \frac{U_0^2k^2/4}{\epsilon+3D_\Omega}}\,\widetilde{\varrho}(\boldsymbol{k},\epsilon - D_\Omega), \tag{A8}$$

where $\widetilde{V}_i(\boldsymbol{k},0) = 0$ has been used and $\widetilde{\varrho}(\boldsymbol{k},0) = (2\pi)^{-1}$, with ϵ being the Laplace variable.

The flux in the Laplace domain $\widetilde{\boldsymbol{J}}(\boldsymbol{k},\epsilon)$ can be directly found from (A8) if one notices that $\widetilde{\boldsymbol{J}}(\boldsymbol{k},\epsilon) = (U_0/2)\widetilde{\boldsymbol{V}}(\boldsymbol{k},\epsilon + D_\Omega)$, thus

$$\widetilde{\boldsymbol{J}}(\boldsymbol{k},\epsilon) = -\frac{U_0^2}{2}i\boldsymbol{k}\frac{1}{\epsilon + D_\Omega + \frac{U_0^2k^2/4}{\epsilon+4D_\Omega}}\widetilde{\varrho}(\boldsymbol{k},\epsilon). \tag{A9}$$

The last equation corresponds to a non-Fickian constitutive relation that considers nonlocal effects, in space and time, as can be directly seen when transformed back to $\boldsymbol{x}$ and t variables, expressly,

$$\boldsymbol{J}(\boldsymbol{x},t) = -\frac{U_0^2}{2}\nabla\int d^2\boldsymbol{y}\int_0^t ds\,\psi(\boldsymbol{x}-\boldsymbol{y},t-s)\varrho(\boldsymbol{y},s), \tag{A10}$$

where the memory $\psi(\boldsymbol{x},t)$ is given by the inverse Fourier transform of

$$\widetilde{\psi}(\boldsymbol{k},t) = e^{-5D_\Omega t/2}\left[\frac{4D_\Omega}{\varpi k}\sin\varpi k + \cos\varpi_k t\right], \qquad \text{(A11)}$$

which is reminiscent of (15), the solution of the telegrapher equation, with $\varpi_k^2 = U_0^2k^2/2 - 9D_\Omega^2/4$. Relation (A10) together with the continuity equation give rise to a nonlocal (in space and time) diffusion-like equation [39,46,47].

[1] P. S. Lovely and F. W. Dahlquist, J. Theor. Biol. **50**, 477 (1975).
[2] T. J. Pedley and J. O. Kessler, Annu. Rev. Fluid Mech. **24**, 313 (1992).
[3] H. C. Berg, *Random Walks in Biology* (Princeton University Press, Princeton, NJ, 1993).
[4] T. Ishikawa and T. J. Pedley, J. Fluid Mech. **588**, 437 (2007).
[5] J. R. Howse, R. A. L. Jones, A. J. Ryan, T. Gough, R. Vafabakhsh, and R. Golestanian, Phys. Rev. Lett. **99**, 048102 (2007).
[6] P. Romanczuk, M. Bar, W. Ebeling, B. Lindner, and L. Schimansky-Geier, Eur. Phys. J. Special Topics **202**, 1 (2012).
[7] E. Lauga and T. Powers, Rep. Prog. Phys. **72**, 096601 (2009).
[8] F. Jülicher and J. Prost, Eur. Phys. J. E **29**, 27 (2009).
[9] F. J. Sevilla and L. A. Gómez Nava, Phys. Rev. E **90**, 022130 (2014).
[10] Y. Fily, A. Baskaran, and M. F. Hagan, Soft Matter **10**, 5609 (2014).
[11] X. Yang, M. L. Manning, and M. C. Marchetti, Soft Matter **10**, 6477 (2014).
[12] J. J. Abbott, K. E. Peyer, M. C. Lagomarsino, L. Zhang, L. Dong, I. K. Kaliakatsos, and B. J. Nelson, Int. J. Robot. Res. **28**, 1434 (2009).
[13] G. Kosa, P. Jakab, G. Szekely, and N. Hata, Biomed. Microdevices **14**, 165 (2012).
[14] W. Gao, R. Dong, S. Thamphiwatana, J. Li, W. Gao, L. Zhang, and J. Wang, ACS Nano **9**(1), 117 (2015).
[15] T. E. Mallouk and A. Sen, Sci. Am. **300**, 72 (2009).
[16] W. F. Paxton, S. Sundararajan, T. E. Mallouk, and A. Sen, Angew. Chem. Int. Ed. **45**, 5420 (2006).
[17] T. Mirkovic, N. S. Zacharia, G. D. Scholes, and G. A. Ozin, ACS Nano **4**, 1782 (2010).
[18] B. ten Hagen, S. van Teeffelen, and H. Lowen, J. Phys. Condens. Matter **23**, 194119 (2011).
[19] V. Lobaskin, D. Lobaskin, and I. Kulic, Eur. Phys. J. Spec Top. **157**, 149 (2008).
[20] S. Ebbens, R. A. L. Jones, A. J. Ryan, R. Golestanian, and J. R. Howse, Phys. Rev. E **82**, 015304(R) (2010).
[21] S. van Teeffelen and H. Lowen, Phys. Rev. E **78**, 020101 (2008).
[22] B. ten Hagen, R. Wittkowski, and H. Lowen, Phys. Rev. E. **84**, 031105 (2011).
[23] M. Sandoval, N. K. Marath, G. Subramanian, and E. Lauga, J. Fluid Mech. **742**, 50 (2014).
[24] T. J. Pedley and J. O. Kessler, J. Fluid Mech. **212**, 155 (1990).
[25] R. N. Bearon and T. J. Pedley, Bull. Math. Biol. **62**, 775 (2000).
[26] M. Enculescu and H. Stark, Phys. Rev. Lett. **107**, 058301 (2011).
[27] J. Palacci, C. Cottin-Bizonne, C. Ybert, and L. Bocquet, Phys. Rev. Lett. **105**, 088304 (2010).
[28] A. Pototsky and H. Stark, Eur. Phys. Lett. **98**, 50004 (2012).
[29] D. Saintillan and M. J. Shelley, Phys. Rev. Lett. **100**, 178103 (2008).
[30] S. Babel, B. ten Hagen, and H. Lowen, J. Stat. Mech. (2014) P02011.
[31] S. Bazazia, J. Buhl, J. J. Hale, M. L. Anstey, G. A. Sword, S. J. Simpson, and I. D. Couzin, Curr. Biol. **18**, 735 (2008).
[32] T. Vicsek, A. Czirok, E. Ben-Jacob, I. Cohen, and O. Shochet, Phys. Rev. Lett. **75**, 1226 (1995).
[33] P. Romanczuk and L. Schimansky-Geier, Phys. Rev. Lett. **106**, 230601 (2011).
[34] X. Zheng, B. ten Hagen, A. Kaiser, M. Wu, H. Cui, Z. Silber-Li, and H. Lowen, Phys. Rev. E **88**, 032304 (2013).
[35] T. D. Frank, Phys. Rev. E **72**, 011112 (2005).
[36] J. Masoliver and K.-G. Wang, Phys. Rev. E **51**, 2987 (1995).
[37] I. Buttinoni, G. Volpe, F. Kümmel, G. Volpe, and C. Bechinger, J. Phys. Condens. Matter **24**, 284129 (2012).
[38] M. J. Schnitzer, Phys. Rev. E **48**, 2553 (1993).
[39] M. E. Cates and J. Tailleur, Europhys. Lett. **101**, 20010 (2013).
[40] S. Goldstein, Quart. J. Mech. Appl. Math. **4**, 129 (1951).
[41] J. Haus and K. Kehr, J. Phys. Chem. Solids **40**, 1019 (1979).
[42] D. Selmeczi, S. Mosler, P. H. Hagedorn, N. B. Larsen, and H. Flyvbjerg, Biophys. J. **89**, 912 (2005).
[43] H.-R. Jiang, N. Yoshinaga, and M. Sano, Phys. Rev. Lett. **105**, 268302 (2010).
[44] K. V. Mardia, Sankhyā, Indian J. Stat. B. **36**, 115 (1974).
[45] B. ten Hagen, S. van Teeffelen, and H. Lowen, Cond. Mat. Phys. **12**, 725 (2009).
[46] A. K. Das, J. Appl. Phys. **70**, 1355 (1991).
[47] V. Kenkre and F. J. Sevilla, in *Contributions to Mathematical Physics: A Tribute to Gerard G. Emch*, edited by T. S. Ali and K. B. Sinha (Hindustan Book Agency, New Delhi, 2007), pp. 147–160.